Langmuir

Article

pubs.acs.org/Langmuir

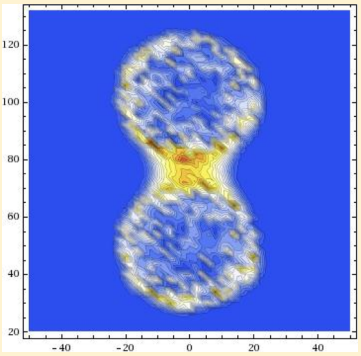
Terms of Use

Influence of Capillary Bridge Formation onto the Silica Nanoparticle Interaction Studied by Grand Canonical Monte Carlo Simulations

Sabine Leroch* and Martin Wendland

Institute of Chemical and Energy Engineering, University of Natural Resources and Life Sciences (BOKU), Muthgasse 107, 1190 Vienna, Austria

ABSTRACT: Adhesion forces between nanoparticles strongly depend on the amount of adsorbed condensed water from ambient atmosphere. Liquid water forms bridges in the cavities separating the particles, giving rise to the so-called capillary forces which in most cases dominate the van der Waals and long-range electrostatic interactions. Capillary forces promote the undesirable agglomeration of particles to large clusters, thereby hindering the flowability of dry powders in process containers. In process engineering macroscopic theories based on the Laplace pressures are used to estimate the strength of the capillary forces. However, especially for low relative humidity and when the wetting of rough or small nanoparticles is studied, those theories can fail. Molecular dynamic simulations can help to give better insight into the water−particle interface. The simulated force versus distance curve as well as adhesion forces and the adsorption isotherm for silica nanoparticles at varying relative humidity will be discussed in comparison to experiments, theories, and simulations.



INTRODUCTION

In many areas of process engineering such as pharmaceutical or food technology industry powders are manipulated in big containers. The flowability of granular dry powders is usually prone to strong shear stresses, which depend on particle shape, particle roughness, adsorbates or chemical impurities on the particle surfaces, and plastic or elastic deformations in the particle surface layers. A principal understanding of the particle interactions on the microscopical scale can help to figure out the causes of the shear stresses to use this knowledge to reduce them. In this paper ultrafine powders in the nanometers range consisting of amorphous silica spheres were studied. Because of the high hydrophilicity of the material, under ambient conditions water vapor is the most frequent chemi- and physisorbed substance on the amorphous silica surface. Moisture drastically changes the adhesion between silica particles, leading to agglomeration of particles into large clusters, thereby hindering the flowability of powders in process containers which is considered undesirable. Hence, it is essential to study particle adhesion for varying relative humidity.

For macroscopic bodies continuum theories based on the Young−Laplace and Kelvin equation are conventionally used to describe the capillary force which originates from liquid bridges that form between the particles by the condensation of water vapor from the atmosphere. The Young−Laplace equation assumes that capillary pressure and surface tension can be defined by two principal radii giving the curvature of the meniscus, while the Kelvin equation requires that the liquid behaves like a continuum on the length scales of the so-called Kelvin length (0.52 nm for water). Over the years the standard equations have been further developed by many groups to account for surface roughness and chemical composition: Rabinovich et al.[1] developed a model to calculate adhesion forces between a particle and a plane with nanoroughness. Butt[2] and Fashchi-Tabrizo et al.[3] presented an analytical model for the adhesion forces between rough particles. Moreover, Butt and Kappl[4] as well as Efremov et al.[5] gave extended reviews of the theoretical treatment of capillary forces along with AFM measurements. Pakarinen et al.[6] numerically calculated the exact meniscus profile between smooth nanoparticles from the Kelvin equation, demonstrating that the standard equations are only applicable for particles larger than 1 μm. Many theories assume that the particle radius or the horizontal extent of the contact area is much larger than the curvature radius of the liquid bridge. Moreover, line tensions caused by the shrinkage or expansion of the liquid meniscus normally not accounted for by many theories are typically in the range of 1 nN like the capillary forces of nanoparticles themselves; i.e., they are not negligible. Because of the introduced approximations in macroscopic theories, they can fail to predict the correct adhesion forces, especially when either the particles themselves or the surface roughness of larger particles are on the nanometer scale. This is especially problematic at low relative humidity when the surfaces are partly wetted by water; then the liquid film is not able to fill the whole contact area between the particles, but rather the water meniscus appears where surface asperities on the particles which are usually on the nanometers scale approach each other. Since gravitational forces play no role for nanoparticle interaction which is dominated by van der Waals and Coulomb forces, the smallness of the investigated particles together with the requirement to determine highly

Received: May 27, 2013
Revised: September 9, 2013
Published: September 9, 2013

 © 2013 American Chemical Society

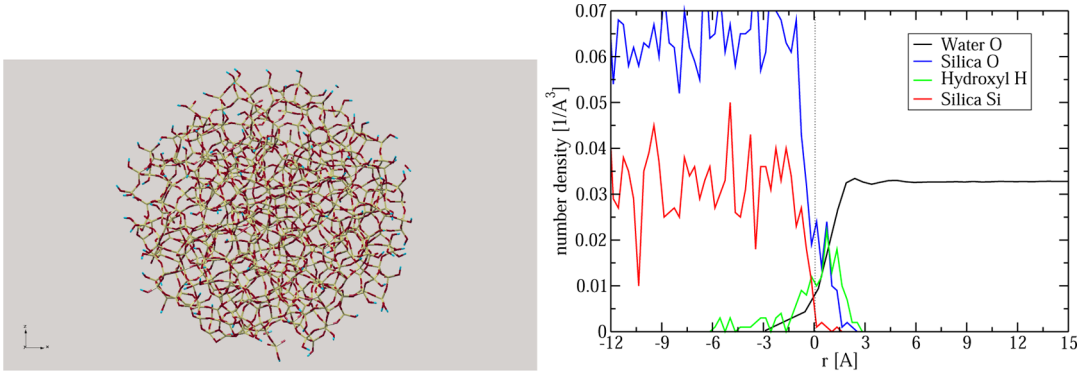


Figure 1. Left: created 4 nm silica particle with silanol density of 4.2/nm^2. Right: number density plot of water on the silica particle, where the vertical line indicates the onset of bulk silica.

accurate adhesion forces predestines the system for molecular dynamic simulations.

To our knowledge the calculation of capillary forces between realistic silica particles has not yet been done by molecular simulation techniques. However, the wetting of crystalline silica plates applying molecular dynamic simulations has been studied by Berendsen and co-workers,[7] who looked at the qualitative agreement of their calculated capillary forces with surface tension forces deduced from macroscopic relations. Cole et al.[8] have carried out molecular dynamic simulations aiming to determine realistic adhesion energies of amorphous silica wafers in dependence of a predefined amount of adsorbed water. Conventionally the Grand Canonical Monte Carlo (GCMC) molecular simulation approach[9] is used to study the behavior of particles under ambient atmosphere. Shinto et al.[10] and Jang et al.[11] used GCMC to simulate force versus distance curves of a humid hydrophilic nanoparticle close to a wall applying simple Lennard-Jones interactions to study the influence of varying hydrophilicity on the adhesion forces. Puibasset and Pellenq[12] have calculated adsorption isotherms for water on different faces of β-cristobalite; moreover, they studied the filling of hydrophilic mesopores[13] using GCMC. Moreover, Ramachandran et al.[14] applied GCMC to calculate adsorption isotherms for conventional water models in silicalite pores, Desbien et al.[15] did the same for zeolite, and Shirono et al.[16] investigated the phase behavior of confined water in silica nanopores. Moreover, Kim et al.[17] have studies the water meniscus formation between an AFM tip and a surface using GCMC simulations. In one of our most recent papers[18] we calculated the forces between silica plates in dependence of the relative humidity applying GCMC simulations, and now we want to adopt the approach for the investigation of humid silica particles.

Amorphous silica has the advantage that it is a well examined substrate. Zhuravlev[19] has given a detailed description of the chemistry of amorphous silica, defining a maximal number of hydroxyl groups on the surface and categorizing them into subgroups according to their chemical reactivity with water molecules. Gösele and Tong[20] have determined surface energies for silica wafer bonding under moist and dry conditions condensing the surface hydroxyls to water, thereby establishing siloxane bonds across the interface. Crack measurements have been done by McKitterick and co-workers.[21] Adhesion energies of contacting silica surfaces exposed to different relative humidity applying crack and atomic force microscopy (AFM) measurements have been proposed by Wan et al.,[22] by Michalske et al.,[23] and by Chikazawa and co-workers,[24,25] who moreover have given adsorption isotherms for water on silica particles with varying silanol density. Lahtinen and co-workers, Butt, Rabinovich et al., and Fashchi-Tabrizi et al.[1−3,26] have measured pull-off forces of silica particles on walls in dependence of relative humidity applying AFM.

To produce force over distance curves of realistic silica nanoparticles, the choice of the atomic interaction potentials is crucial. In the current study the model of Goddard and co-workers[27] was chosen to describe the silicon oxide interactions. It is based on a simple Morse-type short-range potential including the long-range electrostatic interactions via a Coulomb term. Despite its simplicity, it reproduces the amorphous silica structure very accurately and moreover predicts the correct crystal-glass transition temperature. For the water−silica interface we decided to use the conventional Clay force field[28] which has shown[18] a reasonably well described hydrogen-bond network on the silica surface as well as adhesion energies in agreement with experiments.

The paper is organized as follows: First, the simulation details and the creation of the silica nanoparticles are described. This is followed by the results and discussion section where simulated adsorption isotherms, force−distance curves, and pull-off forces in dependence of the relative humidity are presented in comparison to experiments,[1,22,24−26] theories,[2,3] and simulations.[10,11,18] The comparisons are criticaly discussed in the concluding remarks.

METHODS

Creation of the Silica Particles. The silica particles with a diameter of 4 nm are cut out of an amorphous bulk which was created as described in a former paper[18] using the silica potential developed by Demiralp et al.[27] The particles were then annealed for 100 ps at 300 K to reduce the number of dangling bonds on the freshly cleaved surfaces. The structures in terms of radial pair distribution functions and angle distribution functions agree very well with the ones found by Hoang[29] applying the same silica potential. Also, the atomic coordination numbers of silicon and oxide as well as the fraction of silicon and oxide atoms on the surface found in over-, under-, or chemically saturated coordination match well with the values given in ref 29.

To receive a silanol density of 4.2/nm^2 on the surface of the nanoparticles, siloxane bonds (so-called bridging oxygens) have been randomly broken. According to Zhuravlev's model[19] describing the surface chemistry of amorphous silica, the silanol density ranges from 2.6 to 4.6/nm^2, where the silanol groups can be divided into isolated (single silanols), geminal (two hydroxyl groups per silicon), and vicinal or bridged hydroxyl (OH) groups. For a hydroxyl density of 3.55/nm^2

dx.doi.org/10.1021/la402002f | Langmuir 2013, 29, 12410−12420

on silica at room temperature, Zhuravlev has found a portion of isolated, geminal, and vicinal silanols of 0.46, 0.14, and 0.40, respectively, in good agreement with our created particles which can be seen on the left in Figure 1.

Simulation Details. The simulations have been carried out using the open source parallel code LAMMPS.[30,31]

The Clay force field[28] along with the SPC water model was chosen to describe the water−silica and water−water interactions. Although the Clay force field was parametrized for bulk water only and not for its liquid−vapor interface treated in this work, it was shown in a previous paper[18] that the water-mediated interactions are able to reproduce measured surface energies of silica wafers given by experiments of Wan et al.[22] Moreover, we showed[18] that the hydrogen bond structure of water on silica is reasonably well described in comparison to nuclear magnetic resonance measurement[32] and ab initio calculations.[33] Thus, the Clay force field with the parameters given in Table 1 was applied here to study humidity-induced interactions of silica nanoparticles.

Table 1. Nonbonded Force Field Parameters for the Clay Force Field[33] [a]

	q	σ [Å]	ε [kcal/mol]
O_h	−0.95	3.1655	0.1554
H_h	0.425	0.0	0.0
Si	2.1	3.302	1.84×10^{-6}
O_b	−1.05	3.1655	0.1554
O_w	−0.82	3.1655	0.1554
H_w	0.41	0.0	0.0

[a] $U_{ij}^{LJ} = 4\varepsilon_{ij}[(\sigma_{ij}/r_{ij})^{12} - (\sigma_{ij}/r_{ij})^{6}]$, $U_{ij}^{Coul} = q_i q_j/4\pi\varepsilon r_{ij}$. The subscripts b, h, and w stand for bridging oxygens and for atoms part of hydroxyls and water, respectively.

For the Lennard-Jones interactions the standard Lorentz−Berthelot combining rules were used for unlike pairs, where the cutoff was set to 10 Å. The long-range electrostatic interactions have been accounted for applying the particle−particle particle-mesh solver,[34] which is faster than the traditional Ewald summation. The equations of motion are integrated using the velocity-Verlet algorithm with an integration step of 2 fs. All hydrogen bonds and angles have been frozen, applying the SHAKE algorithm.[35]

Since for the Clay force field the parameters for bond stretching and angle bending interactions are only defined for silanol O_s−H_s bonds and Si−O_s−H_s angles, the remaining bond and angle parameters in Table 2 were taken from the CWCA force field.[36] In the course of the simulations the bulk of the particles was kept rigid; only the silanol groups were allowed to move.

In the presence of water vapor in the surrounding atmosphere a certain amount of water molecules is chemisorbed (silanol groups) and physisorbed (hydrogen bonded) on the silica surface. The number of adsorbed water molecules changes in dependence of the air's relative water-vapor pressure P/P_0 (relative humidity) with $P_0 = 0.044$ bar[18] the saturation water-vapor pressure of SPC water and in dependence of the particle separation. To model silica particles under ambient conditions, the grand canonical ensemble is applied since it allows fluctuations in the number of water molecules during the simulation. Along with the grand canonical ensemble the inhomogenous phase given by the adsorbed water molecules on the silica surfaces is in equilibrium with an infinite reservoir of water vapor molecules, imposing its chemical potential and temperature. The saturation pressure of water is extremely low such that only a few water molecules are present in the gas phase of the simulation box; most of them are physically adsorbed on the particle surface. The chemical potential is directly related to the pressure of the surrounding gas phase,[18] such that with the choice of a fixed chemical potential a constant water-vapor pressure and with that a constant relative humidity is set, where the relation between chemical potential and water-vapor pressure was determined in a former publication.[18]

Table 2. Bond Stretching and Angle Bending Parameters for the Clay Force Field[28,36,37] [a]

bonds	K_b	R_0	angles	K_a	r_0
Si−O_b	885.10	1.61	O_b−Si−O_h	153.26	111.09
Si−O_h	428.0	1.61	O_h−Si−O_h	89.62	116.26
O_h−H_h	554.13	1.0	Si−O_h−H_h	30.5	109.47
O_w−H_w	554.13	1.0	H_w−O_w−H_w	45.76	109.47

[a] The bond and angle functions are harmonic with K_b the force constant in kcal/(mol Å^2) and R_0 the equilibrium distance in Å, K_a the force constant in kcal/(mol rad^2), and r_0 the equilibrium angle in degrees.

At the beginning of the simulations a single silica particle was completely dissolved in bulk water to establish an equilibrated water profile from which the number of water molecules adsorbed in the first monolayer (ML) could be deduced. The simulations treating the dissolved particle have been carried out in the isothermal, isobaric (NPT) ensemble[38] for 1 ns at a temperature of 300 K and a pressure of 1 bar, to allow for the adjustment of the simulation box dimensions.

The wetted silica particles were then prepared by removing water molecules from the box of the dissolved particle configuration, leaving only those that form the appropriate portions of water ML around the particles given by the adsorption isotherm corresponding to the selected relative humidity. The adsorption isotherm of SPC water on a single silica particle was calculated applying Grand Canonical Monte Carlo (GCMC) simulations which consisted of at least 600 000 cycles for equilibration followed by a production run of a further 300 000 cycles to deduce the ensemble average for the number of water molecules. At each cycle N particle displacement, rotation, insertion, and deletion attempts have been executed, where N corresponds to the number of water molecules in the simulation box.

When two humid silica particles were brought into closer contact for the force calculations, capillary condensation set in and the number of water molecules were allowed to adjust for at least 600 000 cycles for each selected particle−particle distance. To measure the forces in dependence of particle distance and relative humidity, the silica particles are kept at fixed center of mass distances with respect to each other along the z-axis. The simulations started at a center-of-mass distance of around 70 Å, which was successively reduced by 0.5 Å until the repulsive forces onto the silica particles became dominant. After a stable water meniscus and a constant water molecule number has been established the simulations were continued in the canonical ensemble to save computation time during the collection of the forces, where at each constant distance the system is equilibrated for 1 ns, followed by a production run of 3 ns to collect the center-of-mass forces onto each silica particle.

The mean force

$$F_{AB}(z) = \langle F(z) \rangle = \left\langle \hat{\mathbf{z}} \frac{1}{2}(\vec{F}_A - \vec{F}_B) \right\rangle \quad (1)$$

acting between particles A and B at a certain center-of-mass separation along the z-axis is deduced by an arithmetic average over the total center of mass forces $\vec{F}_A$ and $\vec{F}_B$ collected at the single simulation steps.[18] Assuming ergodicity, the arithmetic average corresponds to the canonical ensemble average denoted by the $\langle\ \rangle$ in eq 1.

To keep the simulation box at a reasonable small size, preserving the performance of the MPI simulations, reflecting hard walls were established perpendicular to the z-axis, each wall 30 Å away from the surface of the closest particle. Thus, the long-range electrostatic interactions have been treaded in the slab configuration, i.e., periodic in the x, y direction and nonperiodic with respect to z.

RESULTS AND DISCUSSION

On the right in Figure 1 the water density profile around a dissolved amorphous silica particle is depicted. To clarify the onset of bulk silica indicated by the vertical line, the number

dx.doi.org/10.1021/la402002f | Langmuir 2013, 29, 12410−12420

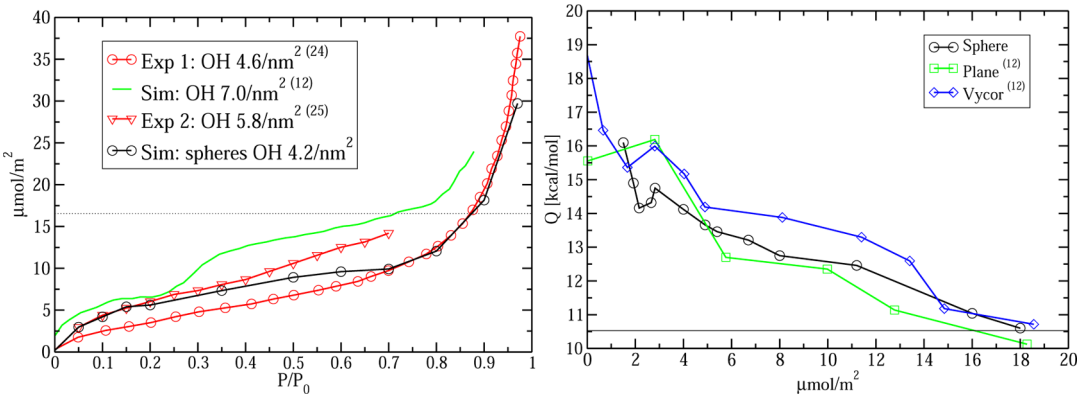


Figure 2. Left: adsorption isotherm of the silica particle with OH density of 4.2/nm^2 in comparison to experiments[24,25] (OH density of 4.6 and 5.8/nm^2) and simulations[12] (OH density of 7.0/nm^2). Right: isosteric heat of adsorption for the nanosphere, in comparison to simulations[12] on Vycor and an amorphous plane.

densities of its atomic contributions are given in the same figure. The origin of the coordinate system has been shifted along the *r*-axis in the following figures depicting the particle forces, such that it coincides with the surface of the first silica particle. As a consequence of the surface roughness of about 2 Å, on the amorphous particle the first water density peak is hardly elevated with respect to the bulk water density. Counting all the water molecules from the interior of the particle to the first minimum in the water density profile in Figure 1 gives a number of water molecules in the first ML of 9.95/nm^2 (compared to the number of 9.6/nm^2 found for a silica plate[18] with an OH density of 3/nm^2). Water molecules are able to penetrate the silica surface up to 3 Å, which could explain the higher number of water molecules in the first monolayer in comparison to early assumptions of 9.52 water molecules/nm^2 made in ref 39 for the quartz surface.

On the left in Figure 2 the adsorption isotherm for water on the silica nanoparticle is presented in comparison to the adsorption isotherm simulated by Puibasset and Pellenq[12] for a silica surface composed of different faces of the β-cristobalite crystal and experiments done by Chikazawa and co-workers[24,25] on nonporous amorphous silica 1.7 μm spheres. The silica plates treaded in ref 12 had the highest hydroxyl density of 7/nm^2 and thus show the largest amount of adsorbed water molecules among the displayed systems in Figure 2. Only for relative humidities above 0.7 the simulated adsorption isotherm agrees with the experimental one measured for a hydroxyl density of 4.6/nm^2, which is comparable with the OH density on the simulated particles. For low and intermediate relative humidity, however, the simulated adsorption isotherm lies above the experimental one and mostly coincides with the asorption isotherm measured for a hydroxyl density of 5.8/nm^2. As already discussed in our last paper,[18] this could be an indication that the silica–water interactions are too strong in the Clay force field while the water–water interactions agree better with experiments. The strong increase in the amount of adsorbed water molecules at low relative humidity explains the large adhesion forces down to very low relative humidity which will be discussed later. For a hydroxyl density as low as 4.2/nm^2 (not shown in Figure 2), Puibasset and Pellenq[12] predicted a water adsorption on amorphous silica plates that starts as from a relative humidity of 0.2, whereas experiments of Fuji et al.[24] show that water already adsorbs strongly at very low relative humidity which was also confirmed by the current simulations.

To have more insight into the water–silica interaction, the isosteric heat of adsorption was calculated on the right in Figure 2 by use of the cross-fluctuations[12]

$$Q_{st} = \frac{\langle UN\rangle - \langle U\rangle\langle N\rangle}{\langle N^2\rangle - \langle N\rangle^2} + RT \qquad (2)$$

with U the potential energy contributions for the water–water and silica–water interactions, N the number of water molecules, R the ideal gas constant, and T the temperature. Within the statistical error of 15% the isosteric heat of adsorption for the amorphous nanosphere agrees well with the one calculated by Puibasset and Pellenq[12] for a Vycor pore and an amorphous surface represented by the superposition of different faces of cristobalite, both at an average silanol density of 7.0/nm^2. The isosteric heat of the particle is in shape similar to the one for Vycor, characteristic for curved surfaces. When around one monolayer (16.5 μmol/m^2) of water is adsorbed, which corresponds to a relative humidity of 0.85, the heat of adsorption becomes nearly equal to the heat of liquefaction of SPC bulk water of 10.5 kcal/mol given by the horizontal line on the right picture in Figure 2. This indicates that the interaction with the silica surface has become negligible as soon as the silica surface is covered with water molecules. For very low relative humidity, on the other hand, the isosteric heat of adsorption for the nanosphere is at least 16 kcal/mol, i.e., well above the heat of liquefaction of SPC bulk water, which characterizes the strong hydrophilicity of the silica particle. Puibasset and Pellenq[12] have shown that for extremely low relative humidity amorphous surfaces can have considerably higher isosteric heat of adsorption than perfect crystal surfaces with comparable silanol density. They argued that in this case the hydrophilicity of the surface is not directly related to the silanol density but rather to locally very favorable arrangements of hydroxyl groups that can maximize the number of hydrogen bonds. On corrugated surfaces the water molecules can easier adsorb on highly energetic sites created by small hole-like defects. Besides surface curvature and defects real[18] amorphous surfaces consist of a considerable large number of low-membered siloxane rings. Bridging oxygens in low-membered rings show a high affinity to hydrogen bond to water molecules if they are close to destabilizing silanol groups. Those single hydrogen-bonded water molecules finally serve as adsorption centers for further water with rising humidity, which leads to the observed steep ascend of the adsorption isotherm in Figure 2 for very low relative humidity.

dx.doi.org/10.1021/la402002f | *Langmuir* 2013, 29, 12410–12420

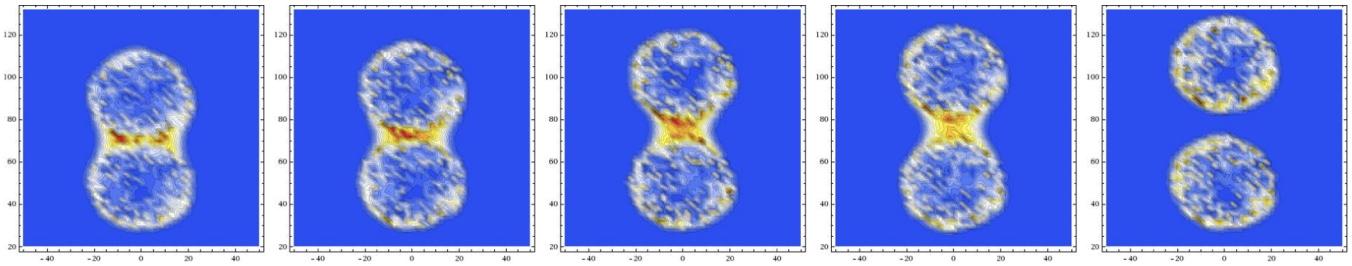


Figure 3. Sketch for the water capillary formation at 0.9 relative humidity for particle distances of 3.0, 7.0, 13.0, 15.0, and 21 Å. Shown are the water densities in small volume elements on the particle surface (the color code ranges from blue (no waters), to white (0.025/Å^3), yellow (0.033/Å^3), and red (0.04/Å^3)). On the vertical axis the particle separation and on the horizontal axis the radial distance from the particle's centers of mass are displayed in Å.

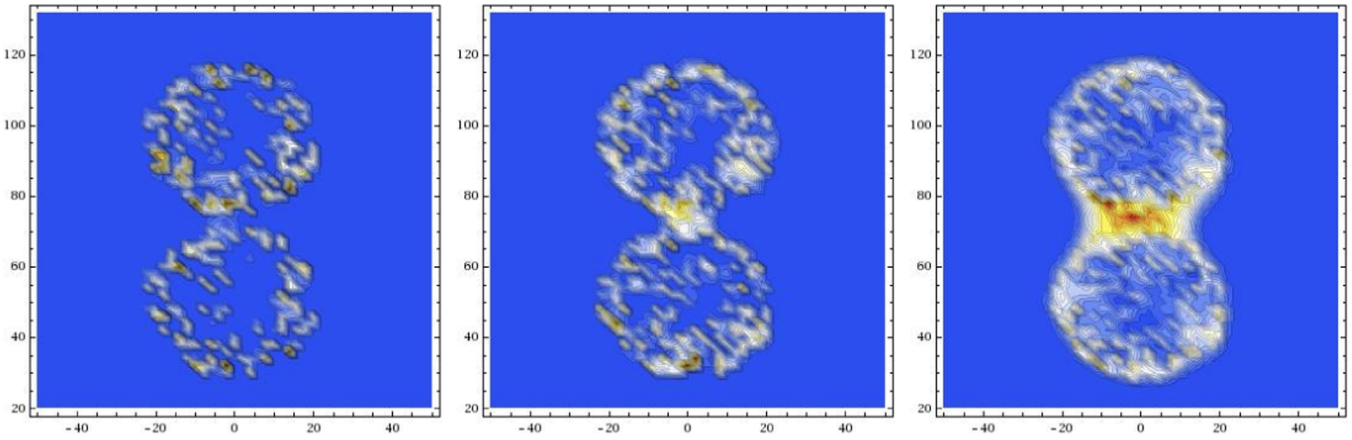


Figure 4. Influence of relative humidity on the size of the water capillary. The relative humidities are 0.1, 0.5, and 0.9 (from left to right), and the particle separation is 9 Å. Shown are the water densities in small volume elements on the particle surface (the color code ranges from blue (no waters) to white (0.025/Å^3), yellow (0.033/Å^3) and red (0.04/Å^3)). On the vertical axis the particle separation and on the horizontal axis the radial distance from the particle's centers of mass are displayed in Å.

When two humid particles approach each other close enough, the adsorbed layers around the particles become instable due to the attractive surface forces, in addition, water from the atmosphere starts to condense into the gap between the particles, which finally leads to the formation of a connecting liquid bridge seen in Figure 3. At every given particle separation the capillary neck between the particles grows in size over time until its curvature has decreased such that evaporation and condensation are in equilibrium. With decreasing particle distance the meniscus becomes broader and less elongated. At narrow gaps finally, water molecules are squeezed out between the particles, and the system cannot compensate for the loss of water molecules by forming a broader meniscus; the water content in the capillary then shrinks.

In Figure 3, water number contour plots for silica nanoparticles exposed to air of 0.9 relative humidity are shown, where the water number is given by the sum of water molecules in small volume elements on the particle surface. The amount of adsorbed water molecules on the noninteracting particles according to the adsorption isotherm in Figure 2 gives 1.15 ML for a relative humidity of 0.9. As one can see, the water molecules are not equally distributed on the silica particle surfaces but concentrated on areas of high hydroxyl density. Even when 16.5 μmol/m^2 is adsorbed, which corresponds to one monolayer of water, small hydrophobic domains on the surface stay free of water molecules while on hydrophilic regions the water molecules start to form a second layer.

In Figure 4, the water meniscus is displayed for different relative humidities of 0.1, 0.5, and 0.9, all at the same particle–particle distance of 9 Å. At low relative humidity no meniscus is formed between the particles, at intermediate relative humidity the particles are bridged by single water molecules forming connecting chains, while at high relative humidity a continuous water meniscus is formed. The onset of capillary condensation at large particle separations is visible in the step in the mean forces acting between the humid particles in Figure 5 for high and intermediate relative humidity. The sudden increase in the attractive forces, resulting from the negative capillary pressure inside the meniscus, pulls the particles together. For small nanoparticles and especially for low relative humidity, one cannot strictly speak of a continuous capillary bridge, but rather of single hydrogen-bonded water chains linking the silanol groups at opposite particles to each other. For decreasing relative humidity the step in the onset of the mean forces at large distances thus disappears and becomes smooth as can be seen in the bottom image of Figure 5.

The mean forces in Figure 5 have been split off into their contributions origin from capillary and direct sphere–sphere interactions. The direct sphere–sphere interactions contribute only up to 7 Å to the total mean forces which are dominated by the capillary forces. The total interactions are of considerably longer range than the forces between dry particles. The range of the capillary forces increases with relative humidity, so for instance in Figure 5 the range is 11, 12, and 21 Å at 0.1, 0.5, and 0.9 relative humidity, respectively.

dx.doi.org/10.1021/la402002f | *Langmuir* 2013, 29, 12410–12420

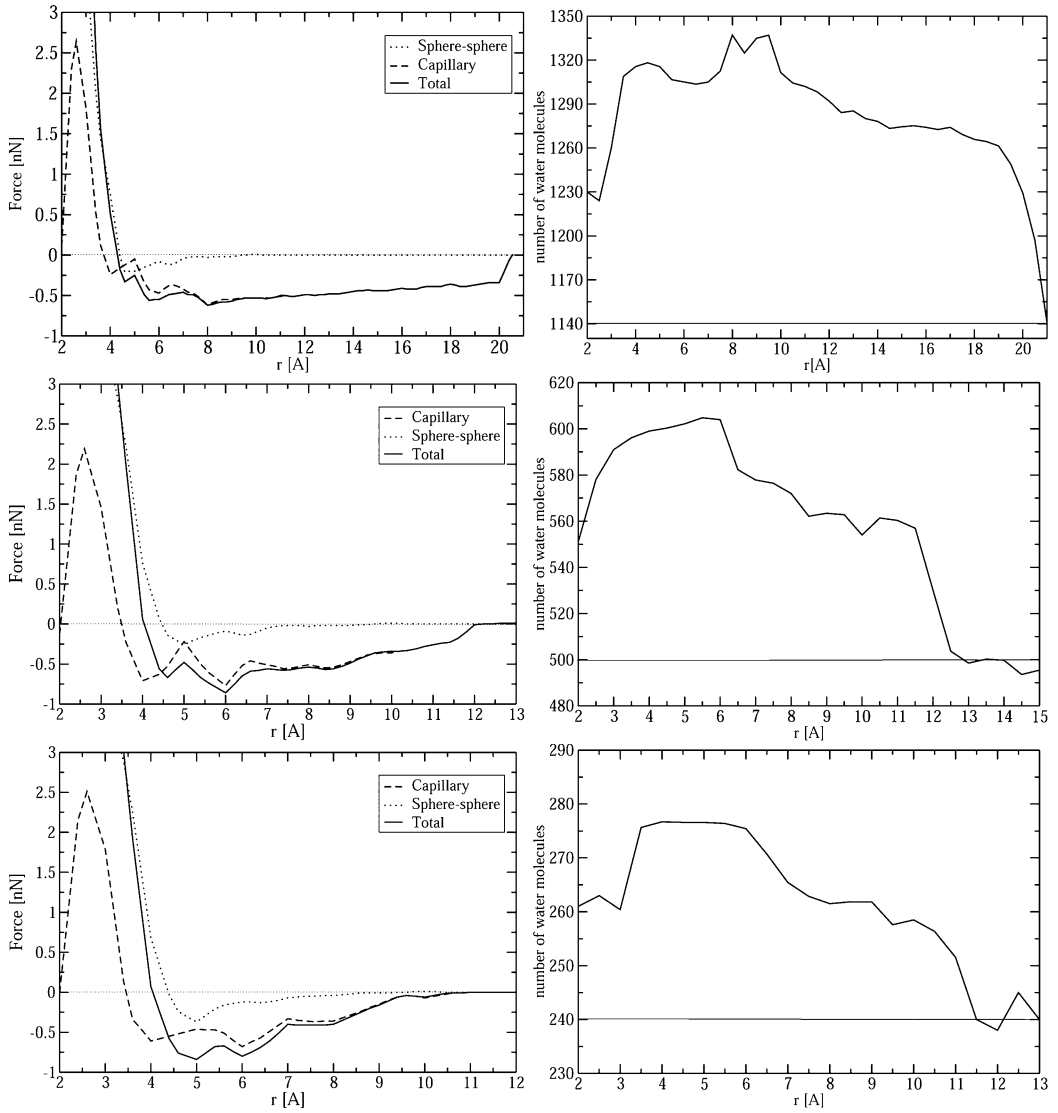


Figure 5. Left: mean force split off into its contributions coming from the capillary and sphere−sphere interactions for 0.9, 0.5, and 0.1 relative humidity (from top to bottom). Right: number of water molecules adsorbed on the particles and in the liquid bridge. The line indicates the number of water molecules on isolated particles.

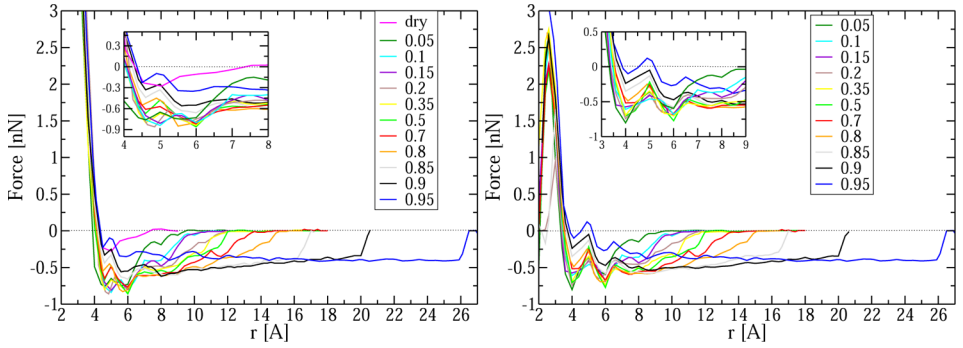


Figure 6. Left: total mean forces for relative humidities between 0 and 0.95. Right: capillary forces for relative humidities between 0.05 and 0.95.

While for large particle separations the mean force is a smooth gently rising function, it exhibits strong oscillations when the surface distances come into the range of a few angstroms. The oscillations at close distances originate from the ordering of the water molecules in the gap between the approaching curved surfaces and show three distinct maxima, at separations of 3.0, 5.0, and 7.0 Å, which indicate water layers formed between the particles. The mean forces are less attractive here since it is not favorable for the particles to penetrate into the water layer. At the equilibrium distance of around 4.0 Å the particles are separated by a single water layer, at 6.0 Å by two water layers, and at 8.0 Å by three water layers,

dx.doi.org/10.1021/la402002f | *Langmuir* 2013, 29, 12410−12420

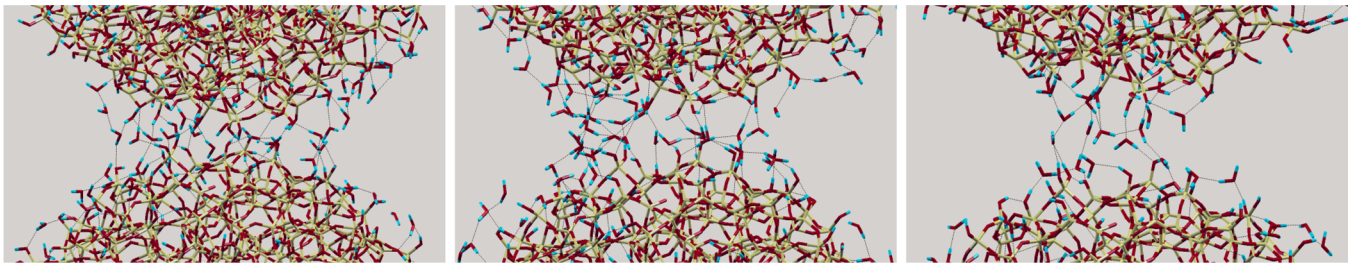


Figure 7. Hydrogen bond network for 0.1 relative humidity at 2.0, 4.0, and 6.0 Å particle distance (from left to right).

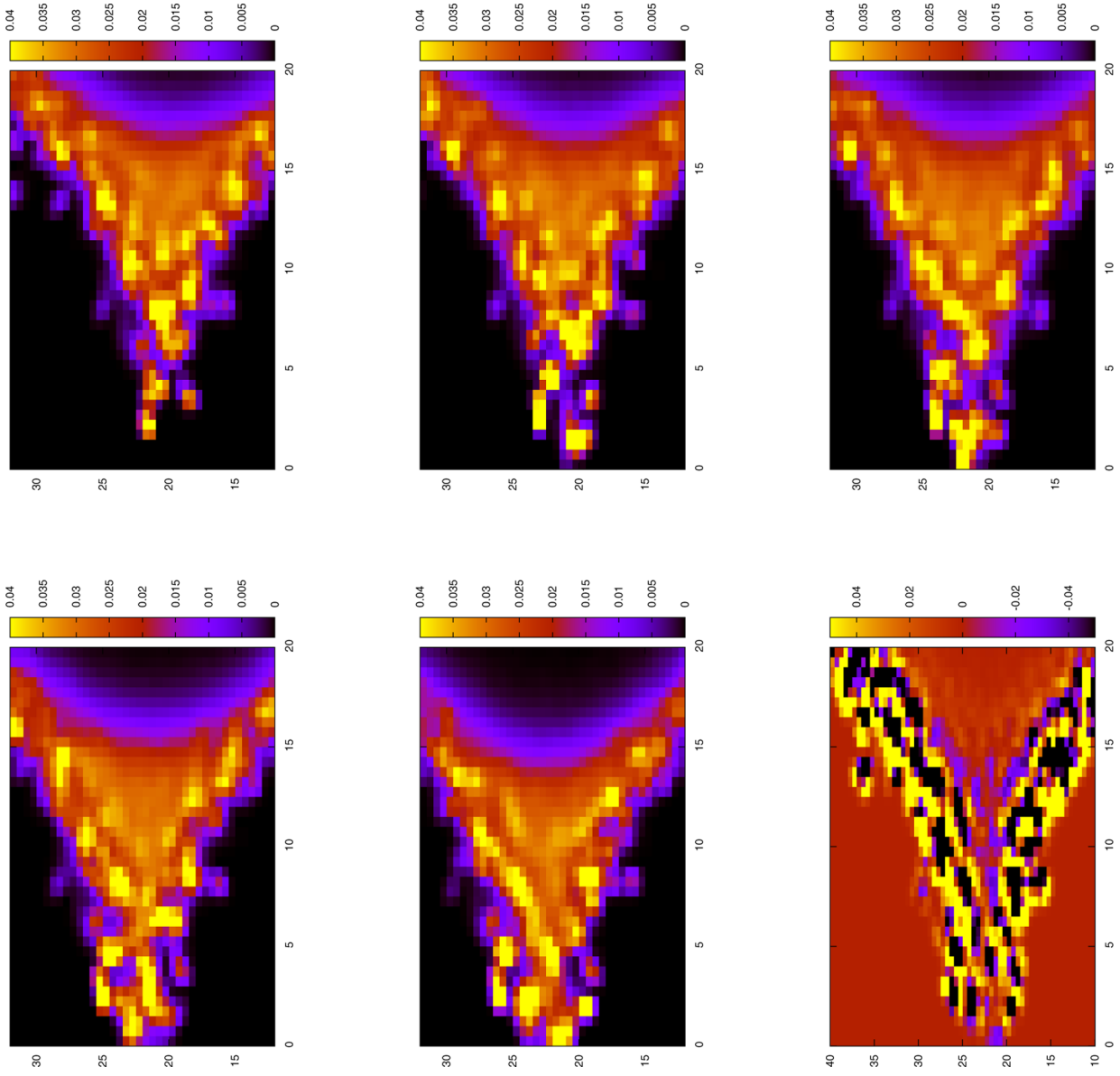


Figure 8. Water density plots (in $1/Å^3$) for 0.9 relative humidity at particle distances of 4.0, 5.0, 6.0, 7.0, and 8.0 Å. The rightmost plot in the second line shows the charge density (in $e/Å^3$) for a distance of 8.0 Å. On the horizontal axis the particle separation and on the vertical axis the radial distance from the particle's centers of mass are displayed in Å.

for instance (as we will discuss in detail later). With increasing relative humidity the mean forces become less attractive at small particle separations because of the increasing amount of water molecules which have to be accommodated between the particles. On the right in Figure 5 the number of adsorbed water molecules in dependence of particle distance and relative humidity is depicted, where the horizontal line in the plots indicates the adsorbed amount of water for isolated particles. As soon as capillary condensation sets in, the number of water molecules jumps due to the formation of a connecting water bridge. Moving the particles closer to each other, the meniscus (or for low relative humidity more and more shorter water

dx.doi.org/10.1021/la402002f | *Langmuir* 2013, 29, 12410−12420

Table 3. Calculated Total and Capillary Pull-Off Forces [mN/m]

rH	dry	0.02	0.05	0.1	0.15	0.2	0.35	0.5	0.7	0.8	0.9	0.95
total	320	687	760	840	800	860	850	860	820	850	620	420
capillary	0	443	640	700	690	750	760	780	750	740	570	420

chains span the gap between the particles) becomes broader, and the number of water molecules constantly rises until at a certain particle distance the removal of water molecules from the region between the particles cannot be compensated by a broadening of the water neck. At that separation the number of water molecules starts to decrease, as can be seen on the right in Figure 5. This separation depends, like the range of the capillary forces, on the relative humidity. For low relative humidity it lies at around 4.0 Å, for intermediate at around 6.0 Å, and for high relative humidity at around 9.0 Å. In agreement with simulations of Shinto et al.,[10] the volume of the water bridge is changing with particle distance; thus, the constant volume approach used in many theories cannot be applied.

To discuss the force curves in dependence of relative humidity, total and capillary mean forces are summarized on the left and right in Figure 6. As can be seen in Figure 5, the capillary forces start to become repulsive with decreasing particle−particle distance at significantly lower distance values than the pure silica−silica forces; i.e., they are still attractive at distances smaller than the equilibrium distance of 4.2 Å for the pure silica−silica interaction. What can be followed from that is that humid particles can approach each other closer than dry ones. In the insets of Figure 6 one can see that the equilibrium distance of the particles is slightly shifted to smaller values for low and intermediate relative humidity in comparison to high relative humidity and dry particles. The increase of the equilibrium distance with rising relative humidity is intuitively clear because of the hydrophilicity of the silica particles which usually leads to good dispersion in water solution. All the forces in Figure 6 show the same trend, irrespective of the relative humidity the force maxima all lie at nearly the same distances of 3, 5, and 7 Å; the forces, however, shifted to higher values with rising relative humidity. The range of the forces becomes longer with increasing relative humidity. This behavior is in qualitative agreement with simulations of Shinto et al.[10] and Jang et al.[11]

The formation of water layers in the meniscus connecting the particles will be discussed in Figure 7. For the system with 0.1 relative humidity one cannot strictly speak of a continuous meniscus but rather of hydrogen-bonded water chains that span the gap between the particles. At a larger distance of 6.0 Å (rightmost plot) water chains consisting of at least (because of the curvature) two water molecules connecting the surfaces by forming hydrogen bonds with silanol groups on opposite particles. Then those hydrogen bonds are broken by moving the particles closer together, squeezing out the water molecules from the region between the particles, visible in the decrease of the attractive forces at 5.0 Å in the bottom plot of Figure 5. At the equilibrium distance close to 4.0 Å at least single water molecules link the particles together; at 2.0 Å finally the surfaces directly approach each other in the center of the contact area seen in the snapshot on the left in the same figure. The water molecules then form a circumventing ring around the particle contact.

For high relative humidity of 0.9 we analyzed the water layers in the meniscus and their correlation to the oscillations in the mean forces in a similar way as has been done by Kim et at.[17] To display the water density and the charge density close to the particles and in the water bridge in Figure 8, the water molecules have been counted in volumes of cylinder rings centered around the particle−particle axis of width dr and height dz of 1 Å, where the density is then gained by dividing the number of water molecules or the sum of the charges by the cylinder ring volume. The densities are shown for particle separations of 4, 5, 6, 7, and 8 Å, corresponding to the minima and maxima of the capillary forces in Figure 5. All the graphs in Figure 8 have in common that the water density is elevated with respect to the water bulk density of 0.033/Å^3 near the surfaces of the particles, while in the interior of the water bridge the water density hardly deviates from the bulk one. This behavior could already be seen in the density profile on the right in Figure 1. With increasing distance from the vertical axis r the number density decreases and vanishes where the cavity opens. For very narrow cavities as for the particle distance of 4 Å the density is zero for small r since a full water layer is not able to be formed in the gap between the particles. For the particle distance of 5 Å two density maxima lying close to 20.36 and 22.7 Å can be seen with a separation between them of 2.34 Å, which is slightly smaller than the water molecular diameter of 2.7 Å, indicating that a second water layer is not yet fully developed. At a distance of 6 Å the maxima lie at 21.6 and 24.3 Å with a difference that corresponds to a water molecular diameter. At 7 Å the maxima can be found at 21.5, 22.8, and 24.9 Å, indicating that a third layer in the middle of the capillary is not yet formed. At 8 Å finally the maxima are at 21.4, 23.6, and 26.23 Å with distance between the maxima of 2.2 and 2.5 Å, indicating the presence of a not yet fully developed third water layer. The charge density in Figure 8 can give information about the orientation of the water molecules in the water bridge. As can be seen the positively charged hydrogen atoms are preferentially orientated toward the particle surface while the oxygens point into the water bridge. For larger distances from the particles the charge distribution becomes nearly uniform, giving evidence that the water molecules adopt no special orientation with respect to the silica surface in the interior of the water meniscus.

Experimentally, the adhesion forces between particles can be determined by atomic force microscopy measurements. The so-called pull-off or adhesion forces are given by the global minimum in the mean forces and correspond to the force dedicated to separate two humid silica particles from their pull-off distance. The pull-off distance gives the location of the global force minimum, so for instance in Figure 5 it is at 8 Å for high, at 6 Å for intermediate, and at 5 Å for low relative humidity, where the pull-off distances for total and capillary forces do not necessarily coincide. The pull-off forces at different water coverage can be seen in Table 3 and Figure 9.

The forces in Figure 9 are normalized with respect to the particle radius R = 20 Å and compared with the Laplace-pressure contribution to the forces in the limit of very small meniscus radius[40]

$$\frac{2F}{R} = 3\pi\gamma \cos\theta \tag{3}$$

dx.doi.org/10.1021/la402002f | Langmuir 2013, 29, 12410−12420

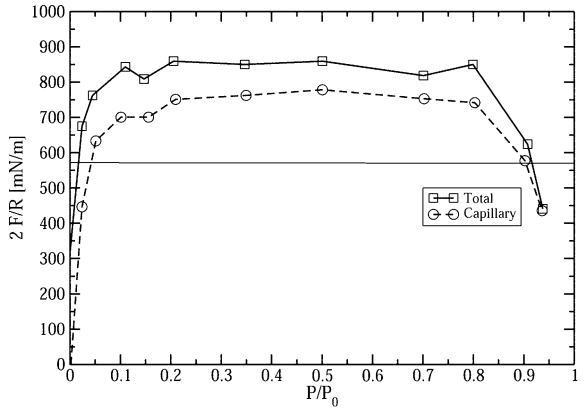


Figure 9. Total and capillary pull-off forces for relative humidities between 0 and 1.

with γ = 73 mN/m the water-vapor surface tension and θ = 30° the contact angle of water on silica. It assumes an adhesion force that is independent of the relative humidity and a particle radius that is much larger than the radius of the mensicus. For a particle radius of 20 Å this is hardly fulfilled. That the adhesion force of nano-sized particles is not independent of humidity has been shown by AFM measurements[26] as well as by more advanced macroscopic theories.[1,6,40] Equation 3 states therefore a crude estimation for the capillary forces and thus conventionally only serves as convergence limit, indicated by the horizontal line, for the adhesion force at high relative humidity. At 0.95 relative humidity the pull-off force, however, falls below this limiting value, which could be caused by the known underestimation of the water surface tension by the SPC water model.

The normalization of the pull-off forces with respect to R is conventionally done in experiments to make the forces independent of particle size. This works fine when the particle radius is at least in the range of several 100 nm;[6] for smaller particles, however, the pull-off forces are still size dependent even after normalization. So, for instance, normalized water-capillary forces calculated by Pakarinen et al.[6] applying a macroscopic model for smooth nanoparticles of different sizes have shown that with decreasing radius the maximum of the pull-off force curve is shifted to lower values and lower relative humidity.

In Figure 9, the total and the capillary part of the pull-off forces are displayed in dependence of the relative humidity. Both curves run through a flat maximum between 0.1 and 0.8 relative humidity, exhibiting smaller pull-off forces for nearly dry and very humid particles. Contact adhesion measurements of Wan et al.[22] gave surface energies between wetted silica plates which are nearly constant over the whole range of investigated relative humidities between 0.05 and 0.95. The surface energy they found was 105 mJ/m^2, which corresponds to an adhesion force between curved surfaces of 990 mN/m applying the Derjaguin equation $2F/R = 3\pi\gamma$, where this approximation relates the surface energy γ between deformable flat surfaces to the forces between spherical particles separated by the same surface to surface distance. Moreover, surface energies for amorphous silica surfaces simulated in a former publication[18] varied between 82 and 100 mJ/m^2 (which translates to particle forces between 772 and 942 mN/m) for relative humidities between 0.8 and 0.3, respectively, which agrees reasonably well with the force values in Figure 9.

Moreover, with respect to principal shape and maximum value of the force–humidity curve good agreement in comparison to AFM experiments and macroscopic theories was achieved. AFM measurements of a silicon nitride tip on a silica wafer under ambient conditions[3] gave a force–humidity curve with a steep maximum of 820 mN/m around 0.7 relative humidity. Moreover, Butt[2] calculated water capillary forces for rough microspheres at zero separation and contact angle with a maximum of around 820 mN/m at very high relative humdity, by describing the roughness of 5 Å by a rectangular asperity distribution. Also, Pakarinen et al.[6] got water capillary forces running through a maximum of 720 mN/m at 0.8 relative humidity applying their model to a hydrophilic smooth 15 nm sphere at a distance of 3 Å from a smooth hydrophilic wall. All those force values lie in the same range as the pull-off forces in Table 3 and Figure 9, certainly with their maximum at different relative humidity than the current simulations suggest.

One may, however, not forget to mention that there are AFM measurements that predict a complete different shape of the force–humidity curve for silica surfaces. So for instance AFM measurements executed by Rabinovich et al.[1] for silica microspheres on a rough silica surface of root-mean-square roughness of 2.2 Å showed a continuous increase of the adhesion force ending in a broad plateau of around 650 mN/m between 0.4 and 0.8 relative humidity; even somewhat smaller maximum adhesion forces have been measured between humid hydrophilic silica nanospheres by Paajaninen et al.[26] Moreover, for relative humidities lower than 0.2 the capillary force vanished completely in those experiments in contradiction to our simulations. Furthermore, adhesion forces measured by Fuji et al.[24] between silica microspheres of varying silanol density (hydrophilicity) gave a completely different shape of the force curve which did not exhibit a maximum or a plateau at a certain relative humidity but instead increased monotonically having a similar shape as the adsorption isotherm in Figure 2.

What can be followed from the aforesaid is that the adhesion force can either increase monotonically, remain relatively constant by encountering a plateau, or run through a maximum with changing relative humidity even on very similar surfaces or particles from the same batch of a nearly monodisperse powder. Besides the chemical heterogeneity of the surface which can lead to variations in the energy of adhesion in dependence of which regions on the two particle surfaces are in direct contact, the roughness has been suggested as cause for the variation. The reason why a force plateau or a maximum in the adhesion force is established with respect to the relative humidity was investigated by molecular dynamic simulations of Jang et al.[11] They changed the hydrophilicity of the tip by varrying its chemical composition and showed that for weakly hydrophilic tips on strongly hydrophilic surfaces the adhesion force is nearly zero for low relative humidity and steadily rises with increasing humidity forming a plateau, while for high hydrophilicity the capillary force is already observable at very low relative humidity and becomes a nonmonotonic function of humidity where the maximum in the adhesion force moves to lower relative humidity. This was also confirmed by simulations with nanoparticles on planes by Shinto et al.[10]

Fashchi-Tabrizi et al.[3] and Pakarinen et al.[6] have shown that moreover, particle size and tip geometry can explain the ambiguity in the shape of the force–humidity curves. Fashchi-Tabrizi et al.[3] tried to reproduce the different shapes of force–humidity curves which they gained from AFM measurements for a silicon nitride tip on a silicon wafer, on a mica surface, and

on an iron particle under ambient conditions, by systematically studying the influence of variations in particle size, roughness, and tip geometry in their theoretical model.

They showed that the curve for a perfectly smooth large sphere on a smooth surface (or a second smooth sphere) is nearly flat down to very low relative humidity, while for very high relative humidity it slowly descends. Only if some surface roughness is included into the model[2] the force–humidity curve gradually decreases for low humidity exhibiting a force maximum, where the region of zero-capillary force increases with higher surface roughness. Besides the surface roughness also the particle size has an effect on the formation of a force maximum. Pakarinen et al.[6] showed that a maximum in the force curve calculated for hydrophilic nanoparticles can be observed only as from a certain particle radius downward and that it moves to lower relative humidity with decreasing radius. Finally, it was shown by Pakarinen et al.[6] and Fashchi-Tabrizi et al.[3] that the particle shape has a major influence on the force–humidity curve. The increase of the adhesion force with relative humidity found by Fuji et al.[24] for instance could be explained by the use of a cone-like instead of a sphere-like tip.[3,6]

To summarize the above, the agreement with AFM meansurements and theoretical predictions is good as far as the principal shape of the force–humidity curve and the value of its maximum are concerned.[3,6] The discrepancies in comparison to some experiments[1,24,26] could be attributed to differences in the hydrophilicity (in terms of surface roughness or chemistry) or geometry between the investigated sample in the lab and simulations. Moreover, it is a size effect since with smaller particle size the maximum of the adhesion force moves to lower relative humidity and lower values[4,6] and the region of zero capillary force at low relative humidity shrinks.

■ CONCLUSION

Adsorption isotherms calculated for silica nanoparticles were nearly in perfect agreement with experiments of Fuji et al.[24] at high relative humidity, while for low relative humidity the amount of adsorped water molecules was considerably higher than in the experiments. This could be attributed to an overestimation of the silica–water interations in the Clay force field. The isosteric heat of adsorption adopts high values for very low humidity, in agreement with other simulations[12] which cannot be explained in dependence of the hydroxyl density, but by surface defects and the presence of low membered siloxane rings typically found on amorphous surfaces which create energetically favorable sites for the adsorption of water molecules which serve as adorption centers for further water with rising relative humidity. Thus, the adsorption isotherm of amorphous surfaces can show a nonzero amount of adsorbed water, even at lower relative pressures than necessary for the water adsorption on perfect crystalline surfaces of comparable OH density. With rising number of adsorbed water molecules the isosteric heat of adsorption decreases, since more and more water molecules hydrogen bind to adsorbed water molecules and not directly to hydroxyls on the silica surface. When around one full monolayer of water covers the particle surface, the heat of adsorption is thus close to the heat of liquefaction of bulk water.

When two particles approach each other close enough to enable capillary condensation, a water bridge is formed between the particles which causes an additional attractive force to the van der Waals interactions. In agreement with other simulations,[10,11] the capillary force becomes longer ranged but gentler in slope with higher humidity and shows oscillations for very small particle distances indicating the layering of water molecules in the interparticle gap. The volume of water in the capillary is not constant as assumed by many theories. It slowly rises with the onset of capillary condensation, runs through a maximum, and finally decays when the broadening of the water bridge with decreasing distance cannot compensate for the number of squeezed out water molecules. For small nanoparticles one cannot speak of a continuous water mensicus but rather of hydrogen-bonded water chains that connect the particles.

The pure silica–silica interactions between dry particles are of considerable shorter range, weaker in magnitude and stronger repulsive at very close contact than the capillary forces. It is thus not surprising that particles under humid conditions can approach each other closer. Moreover, the presence of water has the effect that the particles are much more tightly bound to each other than the same particles in perfect vacuum. Only for very high relative humidity the water layers lead to weaker attractive interactions at close particle approach such that the equilibrium distance shifts to bigger values, which is characteristic for strongly hydrophilic particles in solution.

The forces needed to detach two particles from contact are called pull-off forces, and their strength depends on the relative humidity of the air. Simulated force–humidity curves exhibit a broad maximum at intermediate relative humidities and decrease for very low and high relative humidities. What can be followed by that is that the flowability of nanosilica powders is best for very dry air or in solution, while for low and intermediate relative humidity the particles tend to cluster, which hampers the flowability. As has been demonstrated by Pakarinen et al.[6] and Farshchi-Tabrizi et al.,[3] the observed shape of the simulated force–humidity curve is characteristic for atomistically rough, strongly hydrophilic sphere-shaped bodies. A lower hydrophilicity would shift the force maximum to higher relative humidity or replace it by a force plateau. Moreover, the appearance of a maximum is also a size effect, where an existing maximum moves to lower relative humidity with decreasing particle radius. Regardless of the location of the force maximum and the exact shape of the force–humidity curve many experiments and theories are in reasonable good agreement with our simulated force–humidity curves giving maxima of around 850 mN/m (750 mN/m for the capillary part alone). At very high relative humidity, however, the pull-off force is underestimated by the SPC water model.

■ AUTHOR INFORMATION

Corresponding Author

*E-mail: sabine.leroch@boku.ac.at (S.L.).

Notes

The authors declare no competing financial interest.

■ ACKNOWLEDGMENTS

Financial support by the Fond zur Förderung der wissenschaftlichen Forschung (FWF) under project ID FWF I 498-N19 “Moleculare Structure and Interactions between Particles”, within the priority research programme SPP1486 “Partikel in Kontakt (PiKo)” of the Deutsche Forschungsgemeinschaft (DFG) as well as the allocation of computer time at the Vienna Scientific Cluster (VSC), project ID 70190, is gratefully acknowledged.

REFERENCES

(1) Rabinovich, Y. I.; Adler, J. J.; Esayanur, M. S.; Ata, A.; Singh, R. K.; Moudgil, B. M. Capillary forces between surfaces with nanosclae roughness. *Adv. Colloid Interface Sci.* **2002**, *96*, 213−229.

(2) Butt, H. J. Capillary forces: Influence of roughness and heterogeneity. *Langmuir* **2008**, *24*, 4715−4721.

(3) Farshchi-Tabrizi, M.; Kappl, M.; Cheng, Y.; Gutmann, J.; Butt, H. J. On the adhesion between fine particles and nanocontacts: An atomic force microscope study. *Langmuir* **2006**, *22*, 2171−2184.

(4) Butt, H. J.; Kappl, M. Normal capillary forces. *Adv. Colloid Interface Sci.* **2009**, *146*, 48−60.

(5) Efremov, A. A.; Lytvyn, P. M.; Dyachynska, A. O. A. O. M.; Aleksyeyeva, T. A.; Prokopenko, I. V. Nanoprobe spectroscopy of capillary forces and its application for a real surface diagnostics. *Semicond. Phys., Quantum Electron. Optoelectron.* **2010**, *13*, 111−124.

(6) Pakarinen, O. H.; Foster, A. S.; Paajanen, M.; Kalinainen, T.; Katainen, J.; Makkonen, I.; Lahtinen, J.; Nieminen, R. M. Towards an accurate description of the capillary force in nanoparticle-surface interaction. *Modell. Simul. Mater. Sci. Eng.* **2005**, *13*, 1175−1186.

(7) Wensink, E. J. W.; Hoffmann, A. C.; Apol, M. E. F.; Berendsen, H. J. C. Properties of adsorbed water layers and the effect of adsorbed layers on interparticle forces by liquid bridging. *Langmuir* **2000**, *16*, 7392−7400.

(8) Cole, D. J.; Payne, M. C. Development of a classical force field for the oxidized Si surface: Application to hydrophilic wafer bonding. *J. Chem. Phys.* **2007**, *127*, 204704−12.

(9) Frenkel, D.; Smith, B. *Understanding Molecular Simulation, From Algorithms to Applications*, 1st ed.; Academic Press: Amsterdam, The Netherlands, 1996.

(10) Shinto, H.; Uranishi, K.; Miyahara, M.; Higashitani, K. Wetting-induced interaction between rigid nanoaparticle and plate: A Monte Carlo study. *J. Chem. Phys.* **2002**, *116*, 9500−9509.

(11) Jang, J.; Schatz, G. C.; Ratner, M. A. Capillary force in atomic force microscopy. *J. Chem. Phys.* **2003**, *120*, 1157−1160.

(12) Puibasset, J.; Pellenq, R. J.-M. Water adsorption on hydrophilic mesoporous and plane silica substrates: A grand canonical Monte Carlo simulation study. *J. Chem. Phys.* **2003**, *118*, 5613−5622.

(13) Bonnaud, P. A.; Coasne, B.; Pellenq, R. J.-M. Molecular simulation of water confined in nanoporous silica. *J. Phys.: Condens. Matter* **2009**, *22*, 1−15.

(14) Ramachandran, C. E.; Chempath, S.; Broadbelt, L. J.; Snurr, R. Q. Water adsorption in hydrophobic nanopores: Monte Carlo simulations of water in silicalite. *Microporous Mesoporous Mater.* **2003**, *90*, 293−298.

(15) Desbien, N.; Boutin, A.; Demachy, I. Water condensation in hydrophobic silicalite-1 zeolite: A molecular simulation study. *J. Phys. Chem. B* **2005**, *109*, 24071−24076.

(16) Shirono, K.; Daiguji, H. Molecular simulation of the phase behavior of water confined in silica nanopores. *J. Phys. Chem. C* **2007**, *111*, 7938−7946.

(17) Kim, H.; Smit, B.; Jang, J. Monte Carlo study on the water meniscus condensation and capillary force in atomic force microscopy. *J. Phys. Chem. C* **2012**, *116*, 21923−21931.

(18) Leroch, S.; Wendland, M. Simulation of forces between humid amorphous silica surfaces: A comparison of empirical atomistic force fields. *J. Phys. Chem. C* **2012**, *116*, 26247−26261.

(19) Zhuravlev, L. T. *Colloids Surf., A* **2000**, *173*, 1−38.

(20) Gösele, U.; Tong, Q. Y. Semiconductor wafer bonding. *Annu. Rev. Mater. Sci.* **1998**, *28*, 215−241.

(21) Maszara, W. P.; Götz, G.; Caviglia, A.; McKitterick, J. B. Bonding of silicon wafers for silicon-on-insulator. *J. Appl. Phys.* **1988**, *64*, 4943−4950.

(22) Wan, K.; Smith, D. T.; Lawn, B. R. Fracture and contact adhesion energies of mica-mica, silica-silica, and mica-silica interfaces in dry and moist atmosphere. *J. Am. Ceram. Soc.* **1992**, *75*, 667−676.

(23) Michalske, T. M.; Fuller, E. R. Closure and repropagation of healed cracks in silicate glass. *J. Am. Ceram. Soc.* **1985**, *68*, 586−590.

(24) Fuji, M.; Machida, K.; Takei, T.; Watanabe, T.; Chikazawa, M. Effect of wettability on adhesion force between silica particles evaluated by atomic force microscopy measurements as a function of relative humidity. *Langmuir* **1999**, *15*, 4584−4589.

(25) Takei, T.; Eriguchi, E.; Fuji, M.; Watanabe, T.; Chikazawa, M. Heat of immersion of amorphous and crystalline silicas in water: effect of crystallinity. *Thermochim. Acta* **1997**, *308*, 139−145.

(26) Paajanen, M.; Katainen, J.; Pakarinen, O. H.; Foster, A. S.; Lahtinen, J. Experimental humidity dependency of small particle adhesion on silica and titania. *J. Colloid Interface Sci.* **2006**, *304*, 518−523.

(27) Demiralp, E.; Cagin, T.; Goddard, W. A. Morse stretch potential charge equilibrium force field for ceramics: Application to the quartz-stishovite phase transition and to silica glass. *Phys. Rev. Lett.* **1999**, *82*, 1708−1711.

(28) Cygan, R. T.; Liang, J. J.; Kalinichev, A. G. Molecular models of hydroxide, oxyhydroxide, and clay phases and the development of a general force field. *J. Phys. Chem. B* **2004**, *108*, 1255−1266.

(29) Hoang, V. V. Molecular dynamics simulation of amorphous SiO_2 nanoparticles. *J. Phys. Chem. B* **2007**, *111*, 12649−12656.

(30) http://lammps.sandia.gov/.

(31) Plimpton, S. Fast parallel algorithms for short-range molecular dynamics. *J. Comput. Phys.* **1995**, *117*, 1−19.

(32) Chuang, I. S.; Maciel, G. E. A detailed model of local structure and silanol hydrogen bonding of silica gel surfaces. *J. Phys. Chem. B* **1997**, *101*, 3052−3064.

(33) Skelton, A. A.; Fenter, P.; Kubicki, J. D.; Weslowski, D. J.; Cummings, P. T. Simulations of the quartz(1011)/water interface: A comparison of classical force fields, ab initio molecular dynamics, and X-rax reflectivity experiments. *J. Phys. Chem. C* **2011**, *115*, 2076−2088.

(34) Hockney, R. W.; Eastwood, J. W. *Computer Simulation Using Particles*, 1st ed.; Institute of Physics: New York, 1988.

(35) Ryckaert, J. P.; Ciccotti, G.; Berendsen, H. J. C. Numerical integration of the cartesian equations of motion of a system with constraints: molecular dynamics of n-alkanes. *J. Comput. Phys.* **1977**, *23*, 327−341.

(36) Cruz-Chu, E. R.; Aksimentiev, A.; Schulten, K. *J. Phys. Chem. B* **2006**, *110*, 21497−21508.

(37) Lorenz, C. D.; Crozier, P. S.; Travesset, J. A. A. Molecular dynamics of ionic transport and electrokinetic effects in realistic silica channels. *J. Phys. Chem. C* **2008**, *112*, 10222−10232.

(38) Shinoda, A.; Shiga, S.; Mikami, J. Rapid estimation of elastic constants by molecular dynamics simulation under constant stress. *Phys. Rev. B* **2004**, *69*, 134103−11.

(39) Whalen, J. W. Thermodynamic properties of water adsorbed on quartz. *J. Phys. Chem.* **1961**, *65*, 1676−1681.

(40) Isrealachvili, J. *Intermolecular & Surface Forces*, 2nd ed.; Academic Press: San Diego, CA, 1992.